Open

Oncogene (2012) 31, 4815 - 4827

www.nature.com/onc

ORIGINAL ARTICLE

Endothelial cell dysfunction and cytoskeletal changes associated with repression of p16^{INK4a} during immortalization

C-Y Kan[1,4], VW Wen[1,4], E Pasquier[2], K Jankowski[1], M Chang[2], LA Richards[1], M Kavallaris[2,3] and KL MacKenzie[1]

The immortalization process is a fundamental step in the development of most (if not all) human cancers, including the aggressive endothelial cell (EC)-derived malignancy angiosarcoma. Inactivation of the tumor suppressor p16^{INK4a} and the development of multiple chromosomal abnormalities are features of angiosarcoma that are recapitulated during telomerase-mediated immortalization of human ECs *in vitro*. The present study used a panel of telomerase-immortalized bone marrow EC (BMEC) lines to define the consequences of inactivation of p16^{INK4a} on EC function and to identify molecular changes associated with repression of p16^{INK4a}. In a comparison of two immortalized BMEC mass cultures and six clones, the cell lines that repressed p16^{INK4a} showed a higher rate of proliferation and an impaired ability to undergo morphogenic differentiation and form vessel-like structures *in vitro*. Proteomic comparison of a p16^{INK4a}-negative and a p16^{INK4a}-positive BMEC mass culture at early- and late-passage time points following transduction with telomerase reverse transcriptase (hTERT) revealed altered expression of cytoskeletal proteins, including vimentin and α-tropomyosin (αTm), in the immortal cells. Immunoblot analyses of a panel of 11 immortal clones showed that cells that lacked p16^{INK4a} expression tended to accumulate more dramatic changes in these cytoskeletal proteins than cells that retained p16^{INK4a} expression. This corresponded with aberrant cytoskeletal architectures among p16^{INK4a}-negative clones, which featured thicker actin stress fibers and less fluid membrane ruffles than p16^{INK4a}-positive cells. A direct link between p16^{INK4a} repression and defective EC function was confirmed by analysis of normal cells transfected with small interfering RNA (siRNA) targeting p16^{INK4a}. siRNA-mediated repression of p16^{INK4a} significantly impaired random motility and vessel formation *in vitro*. This report is the first to demonstrate that ECs that repress the expression of p16^{INK4a} are prone to defects in motility, morphogenesis and cytoskeletal organization. These defects are likely to reflect alterations that occur during the development of EC-derived malignancies.

Oncogene (2012) **31,** 4815–4827; doi:10.1038/onc.2011.645; published online 6 February 2012

Keywords: endothelial cell; p16^{INK4a}; TERT; immortalization; cytoskeleton; morphogenesis

INTRODUCTION

Endothelial cell (EC)-derived neoplasias range from benign hemangiomas and intermediate-grade Kaposi's sarcoma to aggressive angiosarcomas, which respond poorly to current treatments.[1,2] These malignancies are characterized by EC hyperproliferation and development of tumorous masses composed of poorly formed vascular structures. Silencing of the gene encoding p16^{INK4a} (*CDKN2A*) by promoter methylation or deletion has been identified as one of the most commonly occurring molecular aberrations in angiosarcoma, affecting approximately 70% of cases.[3,4]

p16^{INK4a} is expressed at low levels in normal ECs and accumulates to very high levels during senescence.[5] It functions as a cyclin-dependent kinase inhibitor that enforces cell-cycle arrest through activation of the retinoblastoma tumor-suppressor protein (pRB).[6] It is broadly accepted that repression of the *CDKN2A* gene contributes to tumorigenesis by enabling cell-cycle progression and promoting excessive proliferation. However, there is also evidence indicating that inactivation of p16^{INK4a} and/or deregulation of pRB contributes to other aspects of the malignant phenotype, such as impaired differentiation, defective mitosis and development of chromosomal abnormalities.[7–10]

Cellular immortalization is a fundamental step in the development of most, if not all, cancers.[11] In 80–90% of human cancers, cellular immortality is underpinned by activation of the telomere-maintenance enzyme telomerase. In contrast to immortal cancer cells, most normal somatic cells, including mature ECs, express very little telomerase and have a limited replicative lifespan as a result of progressive telomere shortening.[12–15] Critically short telomeres activate a TP53-mediated DNA damage signal, which together with concurrent upregulation of p16^{INK4a}, induces cell-cycle arrest and senescence.[16–19] However, in cells that have silenced p16^{INK4a}, cell-cycle arrest may be compromised, resulting in outgrowth of cells with dysfunctional telomeres that promote the development of karyotypic abnormalities.[20–22]

Reconstitution of telomerase activity by constitutive expression of telomerase reverse transcriptase (hTERT) enables normal human ECs to proliferate beyond senescence.[13,14,23] However, reactivation of telomerase does not appear to be sufficient for immortalization of certain types of ECs.[13,24] Our past studies

[1]Cancer Cell Development Group, Children's Cancer Institute Australia, Lowy Cancer Research Centre, University of New South Wales, Randwick, NSW, Australia; [2]Tumour Biology and Targeting Program, Children's Cancer Institute Australia, Lowy Cancer Research Centre, University of New South Wales, Randwick, NSW, Australia and [3]Australian Centre for Nanomedicine, University of New South Wales, NSW, Australia. Correspondence: Dr KL MacKenzie, Cancer Cell Development Group, Children's Cancer Institute Australia for Medical Research, Lowy Cancer Research Centre, University of New South Wales, PO Box 81, Randwick, NSW 2031, Australia. E-mail: k.mackenzie@unsw.edu.au
[4]Joint first authors: These authors contributed equally to this work.
Received 4 August 2011; revised 6 December 2011; accepted 8 December 2011; published online 6 February 2012

have shown that hTERT-transduced, bone marrow-derived microvascular ECs (BMECs) were immortalized with low efficiency and/or following a lag period (crisis), whereas the combination of hTERT and SV40T early region, which disables both the $p16^{INK4a}$/pRB and p53 tumor-suppressor pathways, very efficiently immortalized both BMECs and mammary ECs.[13,24] Many of the BMEC clones that were transduced with hTERT alone and were eventually immortalized were shown to have spontaneously inactivated $p16^{INK4a}$ by methylation of CpG islands.[25] Complex karyotypes developed in the clones that silenced $p16^{INK4a}$ during immortalization as an apparent consequence of telomere dysfunction. It was notable that the karyotypic abnormalities frequently involved loci that are rearranged in angiosarcoma.[4,25-31] Karyotypic complexity, together with observations of frequent *CDKN2A* promoter methylation in hTERT-immortalized BMECs, highlight the relevance of this immortalization model to the development of EC malignancies.

The present study used a panel of hTERT-immortalized BMECs to investigate the way repression of $p16^{INK4a}$ may contribute to EC dysfunction in vascular neoplasias. The results revealed altered expression of cytoskeletal proteins, morphologic changes, impaired motility and defective vessel formation in association with suppression of $p16^{INK4a}$ in human BMECs.

RESULTS

Increased rate of proliferation associated with repression of $p16^{INK4a}$ during BMEC immortalization

Immortalization of the hTERT-transduced BMEC (BMhTERT) lines used in this study was described previously.[13,25] Among this panel of cell lines, expression of $p16^{INK4a}$ mRNA and protein was repressed owing to methylation of the *CDKN2A* promoter, or genetic deletion in 1 of 2 mass cultures and 5 out of 12 BMhTERT cultures[25] (Figure 1). Irrespective of the status of $p16^{INK4a}$ expression, immortalized BMhTERT cells were not capable of anchorage-independent growth and did not form tumors when $\sim 10 \times 10^6$ cells were injected into the hind flank of Balb/c Nude mice.[13] The present study therefore examined other aspects of EC function that may be altered in association with loss of $p16^{INK4a}$ expression and that may less overtly contribute to a neoplastic phenotype.

Over the course of the immortalization process there was no overall pattern of proliferation that distinguished the $p16^{INK4a}$-positive and $p16^{INK4a}$-negative populations (examples provided in Figure 2a). However, among the populations that surpassed 75 population doublings (PDs), which represents greater than twofold lifespan extension, the rate of proliferation of clones that repressed $p16^{INK4a}$ (0.69 ± 0.04 PDs per day) was significantly higher than clones that continued to express $p16^{INK4a}$ (0.46 ± 0.04 PDs per day) ($P < 0.0005$, unpaired Student's *t*-test) (Figure 2b). The greater proliferative rate of the $p16^{INK4a}$-negative clones was also reflected by higher mitochondrial activity, as determined by 3-(4,5-dimethylthiazol-2-yl)-2,5-diphenyltetrazolium bromide (MTT) assay (Figure 2c). Thus, although loss of $p16^{INK4a}$ expression was not associated with a particular growth pattern during immortalization, it did correlate with an increased rate of proliferation in some immortalized populations.

The MTT assay was also used to compare the proliferation of $p16^{INK4a}$-positive and $p16^{INK4a}$-negative BMhTERT cells in the absence of recombinant human fibroblast growth factor-β and vascular EC growth factor (VEGF), with or without 5% bovine serum (Figure 2d). In serum-supplemented medium, withdrawal of human fibroblast growth factor-β and VEGF had very little impact on normal BMECs or BMhTERT clones. However, serum starvation resulted in significantly lower MTT values for each of the three $p16^{INK4a}$-positive and $p16^{INK4a}$-negative BMhTERT cell lines that were assayed, as well as normal BMECs. Overall the data indicated no apparent impact of $p16^{INK4a}$ silencing on the mitogenic requirements of BMhTERT cells.

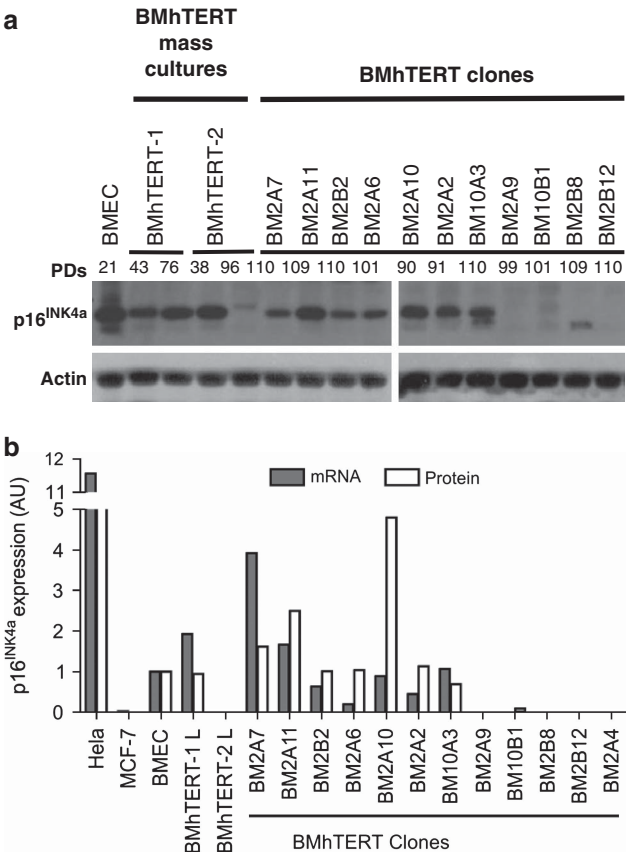

Figure 1. Expression of $p16^{INK4a}$ in BMhTERT cells. (**a**) Immunoblot showing $p16^{INK4a}$ protein expression in BMECs, early- and late-passage BMhTERT-1 and BMhTERT-2 mass cultures, as well as in 11 immortal BMhTERT clones. PDs at the time the cells were assayed are indicated above the gels. (**b**) Quantitation of $p16^{INK4a}$ mRNA and protein expression in BMhTERT cells. mRNA expression was determined by quantitative real-time PCR and normalized to β_2-microglobulin. Protein expression was quantified by densitometry of $p16^{INK4a}$ normalized to actin. The values for $p16^{INK4a}$ mRNA and protein are relative to parental BMECs.

Defective vessel formation by $p16^{INK4a}$-negative BMhTERT cells

To investigate the impact of $p16^{INK4a}$ repression on the unique ability of ECs to undergo morphogenic differentiation and form vessels, parental BMECs and representative $p16^{INK4a}$-positive and $p16^{INK4a}$-negative BMhTERT cell lines were cultured on Matrigel for 6 h. The relatively short duration of this assay was sufficient for control BMECs to undergo morphogenic differentiation and reorganize to form enclosed polygonal structures with anastomosing cords (representing vessel formation), yet was brief enough to be independent of the influence of proliferative rate and increasing cell numbers. In this assay, all four $p16^{INK4a}$-positive BMhTERT immortal cell lines formed vessel-like structures that were morphologically indistinguishable from the structures formed by parental BMECs (Figure 3a). There was no significant difference in the number of enclosed structures generated by immortal BMhTERT cell lines that retained $p16^{INK4a}$ expression compared with control BMECs (Figure 3b). By contrast, 3 out of 4 $p16^{INK4a}$-negative BMhTERT cell lines (BMhTERT-2L mass culture, BM2B8 and BM2B12) were ineffective in the vessel formation assay, producing significantly fewer vessels than normal BMECs and congregating as clumps ($P < 0.01$ for each cell line compared with BMECs; Dunnett's multiple comparison test). One $p16^{INK4a}$-negative BMhTERT clone that retained angiogenic potential, BM2A9, was an exception in this assay (discussed further below).

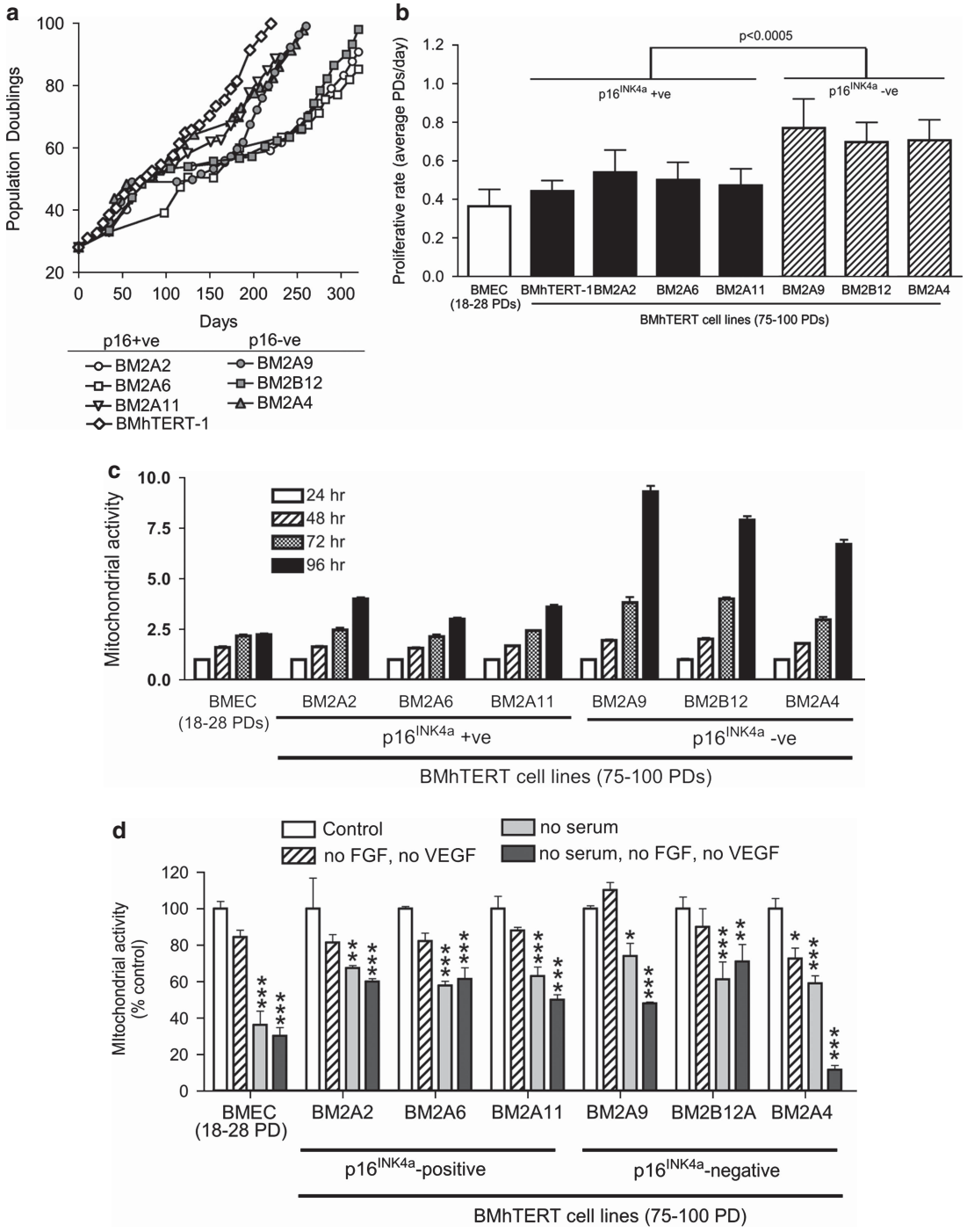

Figure 2. Immortal BMhTERT cells lacking $p16^{INK4a}$ expression have a higher proliferative rate than BMhTERT cells that retained $p16^{INK4a}$ expression. (**a**) Long-term proliferation of BMhTERT-1 mass culture, and representative BMhTERT clones that retained $p16^{INK4a}$ expression (BM2A2, BM2A6 and BM2A11) and clones that repressed $p16^{INK4a}$ expression during immortalization (BM2A9, BM2B12 and BM2A4). (**b**) Average rate of proliferation of normal BMECs, BMhTERT-1 mass culture and representative BMhTERT clones. The values are mean PDs per day ± s.e.m. calculated from at least six time points between 75 and 100 PDs. The *P*-value was generated by comparison of the $p16^{INK4a}$-positive and $p16^{INK4a}$-negative BMhTERT cultures by unpaired Student's *t*-test. (**c**) BMhTERT cells and BMECs were seeded at 3000 cells per well and mitochondrial activity was measured by MTT assay. Values are means ± s.e.m. normalized to the 24-h time point and reflect the proliferation of each cell line. (**d**) BMECs and BMhTERT cells were seeded in 96-well plates in full-factor EGMT-2-MV medium, including 5% fetal bovine serum, recombinant human fibroblast growth factor-β and VEGF. Twenty-four hours later, the medium was changed to either fresh full-factor medium (control) or medium with or without recombinant human fibroblast growth factor-β and VEGF, and/or with or without 5% bovine serum. The MTT assay was performed after a further 96-h incubation. Values were normalized to control conditions. Means and s.e.m. were calculated from duplicates in three independent experiments. $^{*}P < 0.05$; $^{**}P < 0.01$; $^{***}P < 0.001$, determined by two-way analysis of variance with comparison to control conditions using Bonferroni post tests.

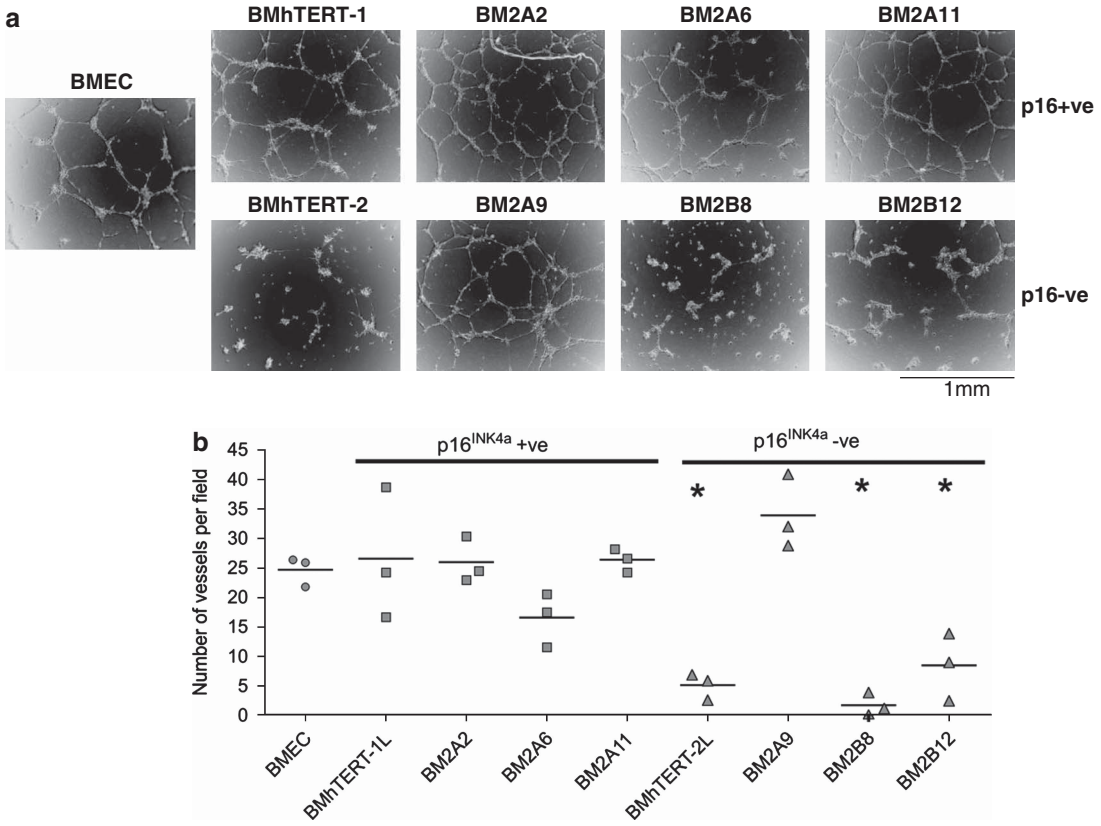

Figure 3. Impaired vessel formation by p16^{INK4a}-negative BMhTERT cells. (**a**) Photomicrographs illustrating the development of vessel-like structures in Matrigel. The photomicrographs were taken using a $\times 5$ objective 6 h after seeding BMECs and BMhTERT cells in Matrigel medium. (**b**) Graphical representation of the number of vessel-like structures (closed polygons) per microscopic field. The values are the average number of vessels per field, enumerated over 10 fields from three independent experiments. * indicates $P<0.01$ in Dunnett's multiple comparison test of BMhTERT cell lines with normal BMECs.

Molecular comparison of p16^{INK4a}-positive and p16^{INK4a}-negative BMhTERT cells

To identify molecular alterations associated with loss of p16^{INK4a} expression, a four-way comparison of the proteomes of BMhTERT-1 (retained p16^{INK4a} expression) and BMhTERT-2 (repressed p16^{INK4a}) mass cultures at early and late stages of the immortalization process were performed using two-dimensional difference in gel electrophoresis (2D DIGE). Protein samples labeled with Cy3- and Cy5-fluorescent dyes, and mixed with a Cy2-labeled internal standard, were separated in six 2D-PAGE gels (Table 1, and Figures 4a and b). Protein spots with differential abundance of at least 1.6-fold were organized into a Venn diagram (Figure 4c). Substantially more proteins were found to be differentially expressed during immortalization of the BMhTERT-2 culture, which repressed p16^{INK4a}, compared with the BMhTERT-1 culture that retained p16^{INK4a} expression. Whereas 43 proteins were differentially expressed in late- versus early-passage BMhTERT-2 cells (BMhTERT-2E versus BMhTERT-2L; Figure 4c, yellow circle), only seven differentially expressed proteins were identified in the comparison of early- and late-passage BMhTERT-1 cells (BMhTERT-1E versus BMhTERT-1L; Figure 4c, red circle). Thirty-two of the 43 proteins that were altered during immortalization of the BMhTERT-2 mass culture (BMhTERT-2E versus BMhTERT-2L) also differed in the comparison of the two immortal mass cultures (BMhTERT-1L versus BMhTERT-2L) (Figure 4c, intersection of blue and yellow circle), indicating a specific association between these 32 proteins and immortalization of the BMhTERT-2 culture, which repressed p16^{INK4a} expression.

After staining with SYPRO Ruby (Figure 4b), proteins of interest were excised from gels under ultraviolet light and analyzed by matrix-assisted laser desorption ionization mass spectrometry (MALDI-MS). Among the 32 proteins that were exclusively associated with immortalization of BMhTERT-2 and repression of p16^{INK4a}, 10 were successfully identified by MALDI-MS (Table 2). These included four cytoskeletal proteins (vimentin #413, macrophage capping protein #599, α-tropomyosin (αTm) #732 and myosin regulatory light chain 2 #1064), two metabolic proteins (L-lactate dehydrogenase B chain and glutathione-*S*-transferase P (GSTPi)) and four additional proteins with various known and unknown functions ((hematopoietic lineage cell-specific protein (HCLS1), testis-specific Y-encoded protein 1 (TSPY1), charged multivesicular body protein 4b and Annexin A4).

Three protein alterations were identified that were commonly altered during immortalization of both BMhTERT-1 and BMhTERT-2 mass cultures (Figure 4c, intersection of red and yellow circles).

Table 1. Experimental design of 2D DIGE analysis of BMhTERT mass cultures

	Cy2	*Cy3*	*Cy5*
Gel-1	Std	BMhTERT-1E (43 PDs)	BMhTERT-1L (76 PDs)
Gel-2	Std	BMhTERT-1E (43 PDs)	BMhTERT-2E (38 PDs)
Gel-3	Std	BMhTERT-2E (38 PDs)	BMhTERT-2L (96 PDs)
Gel-4	Std	BMhTERT-1L (76 PDs)	BMhTERT-2L (96 PDs)
Gel-5	Std	BMhTERT-1L (76 PDs)	BMhTERT-2E (38 PDs)
Gel-6	Std	BMhTERT-2L (96 PDs)	BMhTERT-1E (43 PDs)

Abbreviations: BMhTERT, hTERT-transduced BMEC; 2D DIGE, two-dimensional difference in gel electrophoresis.

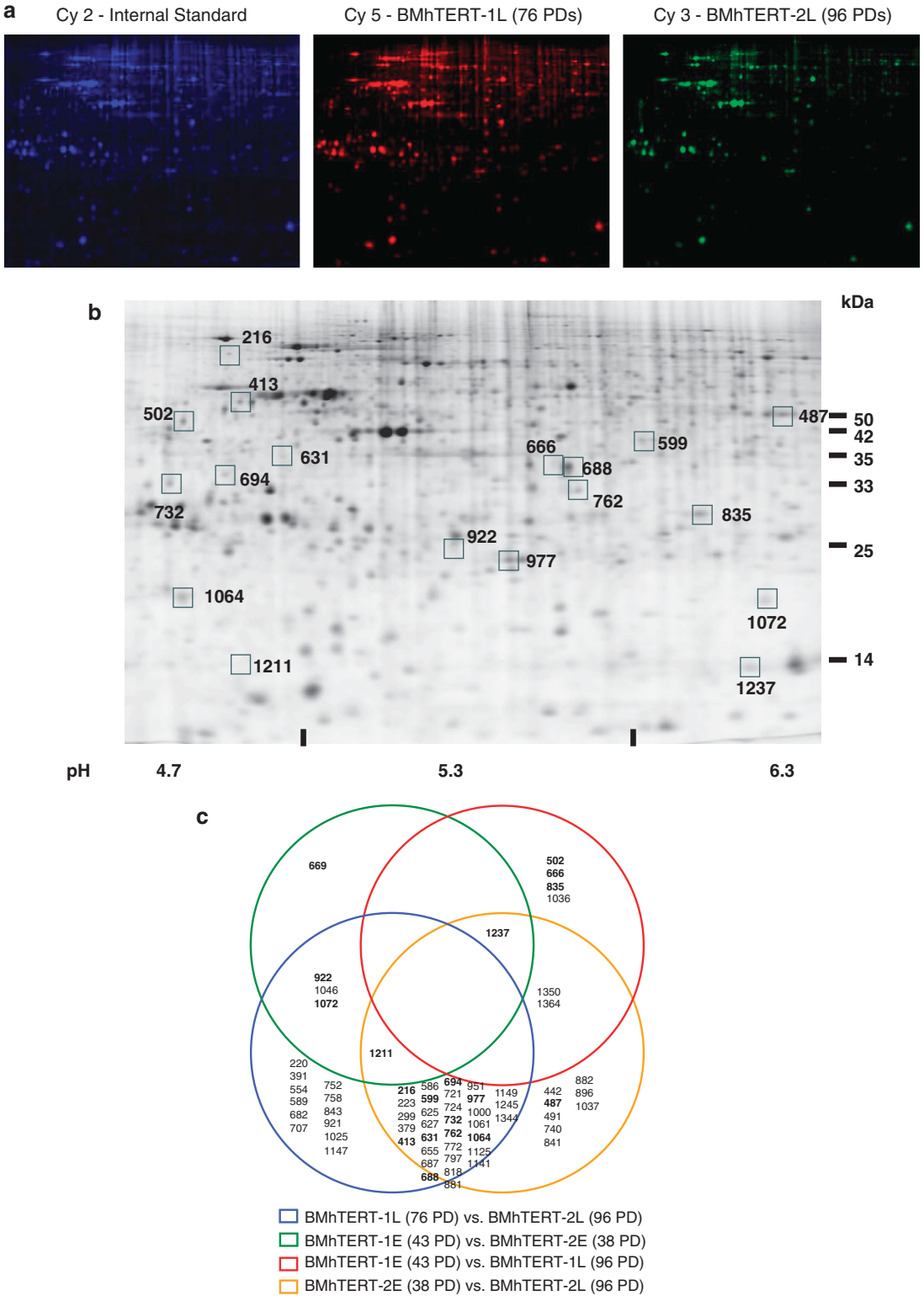

Figure 4. Proteomic alterations during immortalization of BMhTERT cells. Protein lysates from early- and late-passage BMhTERT-1 and BMhTERT-2 cultures were labeled with Cy3 and Cy5 fluorescent dyes. Combinations of the labeled samples, and a Cy2-labeled internal control, were run on six 2D DIGE gels (Table 1). (**a**) A representative 2D DIGE gel (gel #4 in Table 1) showing total cellular proteins in BMhTERT-1L and BMhTERT-2L labeled with Cy5 and Cy3 fluorescent dyes, respectively, and an internal standard labeled with Cy2. Labeled protein spots were detected using the Typhoon imager. (**b**) A representative 2D DIGE gel (gel #4) stained with SYPRO Ruby showing total cellular protein from late-passage BMhTERT-1 and BMhTERT-2 mass cultures, and an internal control. Protein spots of interest (boxed) were excised from SYPRO Ruby-stained gels and identified by MALDI-MS. Protein size estimates in kDa are indicated on the right of the gel. (**c**) A Venn diagram highlighting proteomic changes that occurred during immortalization of the BMhTERT-1 and BMhTERT-2 mass cultures. Statistical analysis of differential protein abundance was calculated using the DeCyder 2D software V4.0, using the Cy2-labeled reference sample as a normalization control. The diagram shows identification numbers of proteins with an abundance of more than 1.6-fold compared with at least one of the other samples. The colored circles delineate the sample comparisons indicated in the legend.

Table 2. Identification of proteins of interest by MALDI-MS

Spot ID[a]	*Gene name*	*Protein name*	*Sequence coverage %*[b]	*MW (kDa)*[c]	*PI*[c]	*Primary accession number*[d]	*Protein abundance*[e]				*Functional classification*	*Locus*
							BMhTERT-1		*BMhTERT-2*			
							Early	*Late*	*Early*	*Late*		
BMhTERT-1E vs BMhTERT-2E: Differentially expressed in BMhTERT-1 and BMhTERT-2 mass cultures prior to immortalization												
922	UCHL1	Ubiquitin carboxyl-terminal hydrolase isoenzyme L1	56	25	5.3	P09936	0.095	0.075	−0.16	−0.18	Protein degradation	4p14
1211	TUBB6	Tubulin β-6 chain (tentative match)	13	50	4.8	Q9BUF5	−0.26	−0.25	0.08	0.5	Cytoskeleton regulation	18p11.21
BMhTERT-1E vs BMhTERT-1L: Altered during immortalization of BMhTERT-1 mass culture												
502	VIM	Vimentin	73	53	5.1	P08670	0.11	−0.19	0.13	−0.04	Cytoskeleton regulation	17q12.3
666	TALDO1	Transaldolase	27	38	6.4	P37837	−0.13	0.08	0.01	0.01	Pentose phosphate pathway enzyme	11p15.5-p15.4
835	GSTO1	Glutathione transferase ω-1	40	28	6.2	P78417	−0.13	0.09	0.02	0.09	Metabolism	10q25.1
BMhTERT-2E vs BMhTERT-2L: Differentially expressed during immortalization of BMhTERT-2 mass culture **Also differentially expressed in BMhTERT-2L compared with BMhTERT-1L*												
487	EEF1G	Elongation factor-1 γ	31	50	6.3	P26641	0.05	−0.12	0.02	−0.3	Translation elongation	11q12.3
*216	HCLS1	Hematopoietic lineage cell-specific protein	28	54	4.7	P14317	−0.13	−0.13	0.05	0.3	Signal transduction, gene regulation	3q13
*413	VIM	Vimentin	64	53	5.1	P08670	0.11	0.1	−0.07	−0.34	Cytoskeleton regulation	17q12.3
*599	CAPG	Macrophage capping protein	45	38	5.9	P40121	−0.05	0.08	0.08	−0.22	Cytoskeleton regulation	2p11.2
*631	TSPY1	Testis-specific Y-encoded protein 1	30	35	5.2	Q01534	−0.15	−0.07	−0.15	0.36	Unknown	Yp11.2
*688	LDHB	L-lactate dehydrogenase B chain	44	36	5.7	P07195	0.05	0.05	0.03	−0.15	Metabolism	12q12.2-p12.1
*694	CHMP4B	Charged multivesicular body protein 4b	35	25	4.8	Q9H444	−0.06	−0.06	−0.06	0.32	Protein transport	20q11.22
*732	TPM1	Tropomyosin 1 (α)	41	33	4.7	P09493	−0.17	−0.31	−0.27	0.6	Cytoskeleton regulation	15q22.1
*762	ANXA4	Annexin-A4	61	36	5.9	P09525	−0.04	0.04	0.04	−0.18	Exocytosis regulation	2p13
*977	GSTP1	Glutathione-*S*-transferase P	56	23	5.4	P09211	−0.01	−0.01	−0.01	0.21	Metabolism	11q13
*1064	MRLC2	Myosin regulatory light chain 2, non-sarcomeric	52	20	4.7	P19105	0.06	0	0	0.27	Cytoskeleton regulation	18p11.31

Abbreviations: BMhTERT, hTERT-transduced BMEC; MALDI-MS, matrix-assisted laser desorption ionization mass spectrometry. [a]Spot numbers were generated by the DeCyder 2DDIGE analysis software. [b]Sequence coverage % is the proportion of amino-acid sequence matched to the indicated protein. [c]Theoretical molecular weight (MW) and isoelectric point (PI) of the identified protein in the database. [d]SwissProt accession number, accessible at www.expasy.org. [e]Protein abundance value was determined using the DeCyder image analysis program.

However these proteins could not be identified by MS, presumably owing to their low abundance. In addition to these three proteins, a vimentin isoform (#502) also appeared to be downregulated in both BMhTERT-1L and BMhTERT-2L, although the values did not reach statistical significance (Table 2). The other vimentin isoform identified in these analyses (#413), which had a molecular mass approximating that of the most studied form of vimentin (57 kDa), was of relatively low abundance in the

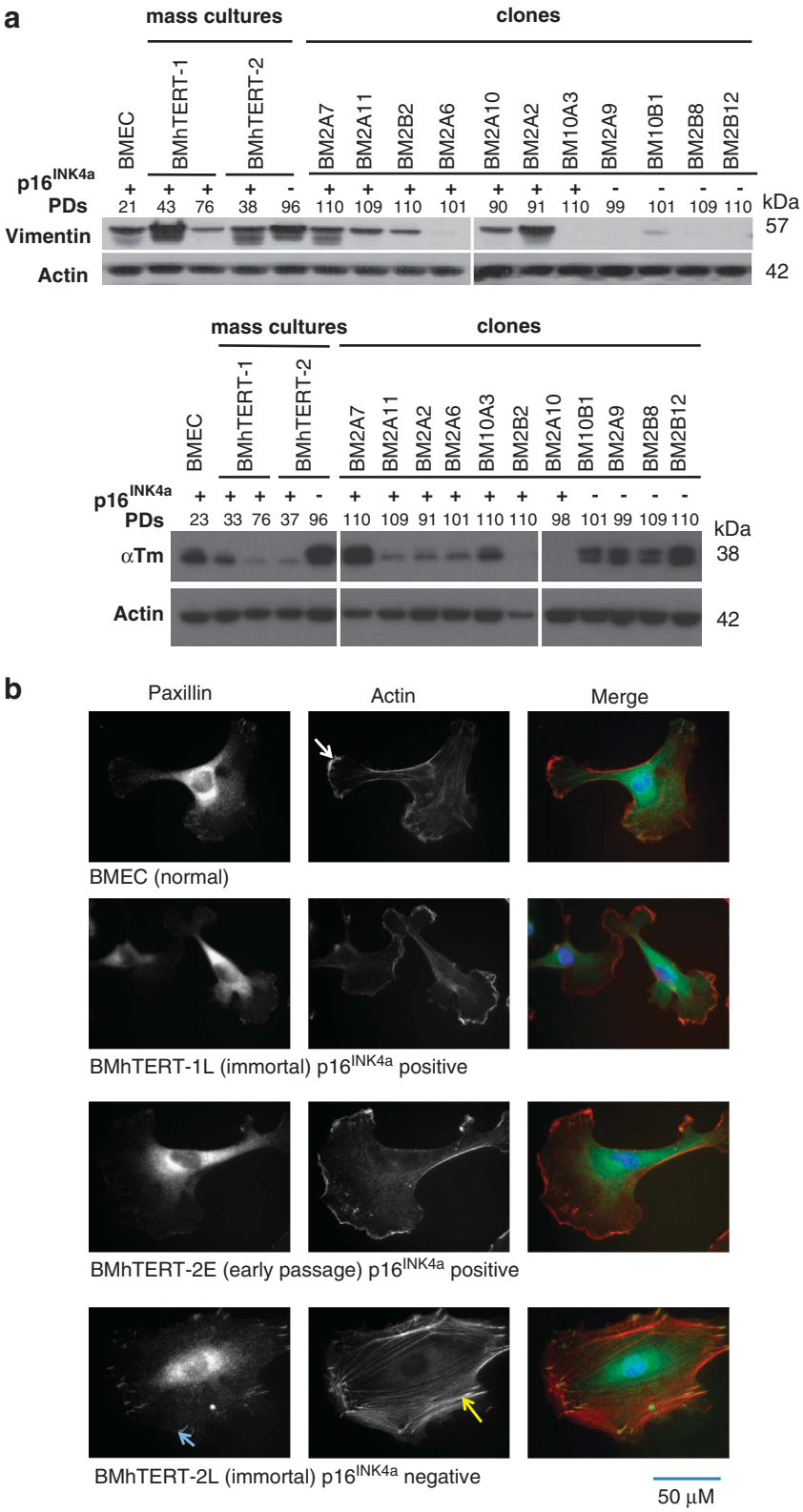

Figure 5. Alterations in vimentin and αTm isoforms, and the altered cell cytoskeleton, of $p16^{INK4a}$-negative immortal BMhTERT cells. (**a**) Immunoblot of BMECs, early- and late-passage BMhTERT-1 and BMhTERT-2 mass cultures, as well as 11 immortal BMhTERT clones. The top panel shows hybridization with antibodies for vimentin and the bottom panel shows hybridization with an antibody specific for αTm. Actin was used as a loading control for both gels. PDs at the time the cells were assayed are indicated above the gels. (**b**) Immunofluorescence staining with paxillin antibody for visualization of focal adhesions (green), phalloidin–Alexa 568 (red) for actin and DAPI (blue). The stained cells were photographed using a ×63 objective.

BMhTERT-2E culture and was further downregulated in the BMhTERT-2L culture. Thus there was a general tendency for vimentin isoforms to be downregulated during immortalization.

Overall, the proteomic analyses revealed that at least 50 proteins were differentially expressed during immortalization of the BMhTERT-1 and BMhTERT-2 mass cultures, with 32 of these being specifically associated with immortalization of the mass culture that repressed $p16^{INK4a}$ and a total of 14 being identified by MALDI-MS. Cytoskeletal proteins featured among the proteins that were altered during immortalization of the BMhTERT-2 culture, which repressed $p16^{INK4a}$ expression.

Alterations in vimentin and Tm isoforms in $p16^{INK4a}$-negative BMhTERT cell lines

Where suitable antibodies were available, immunoblot analysis of 11 BMhTERT clones, as well as early- and late-passage BMhTERT-1 and BMhTERT-2 mass cultures, was performed to validate the 2D DIGE proteomic analysis. Immunoblot analysis of GSTPi and HCLS1 (spot # 216 and 977, respectively) corresponded with the 2D DIGE protein abundance data, showing moderate elevation in late-passage BMhTERT-2 cells relative to early-passage BMhTERT-2 (Supplementary Figure 1 and Table 2). However, these proteins were not consistently elevated across the panel of $p16^{INK4a}$-negative immortal clones in comparison with normal BMECs (Supplementary Figure 1).

Consistent with the detection of vimentin variants by 2D DIGE, immunoblotting using a vimentin antibody revealed multiple bands (at least three) in early-passage BMhTERT cells, as well as normal BMECs (Figure 5a, upper panel). The apparent molecular weight of the most prominent band on the vimentin immunoblot approximated 57 kDa, which corresponded with spot #413 on the 2D DIGE gel. However, whereas 2D DIGE indicated that vimentin #413 was downregulated in BMhTERT-2 cells (Table 2), the immunoblot showed downregulation of the 57-kDa species in the BMhTERT-1 mass culture and not in BMhTERT-2. Nevertheless, the overall results for the immunoblot analysis across the panel of cell lines was consistent with the tendency shown by the proteomics for downregulation of vimentin isoforms, particularly lower molecular weight isoforms, in immortal cells relative to early-passage BMhTERT cultures and normal BMECs. In total, at least 8 out of 13 immortal cultures showed lower expression of one or more vimentin isoforms, with vimentin barely detectable in 4/5 $p16^{INK4A}$-negative cell lines (BM2A9, BM10B1, BM2B8 and BM2B12) and 2/8 $p16^{INK4a}$-positive cell lines (BM2A6 and BM10A3) (Figure 5a, upper panel).

Immunoblot analysis of αTm confirmed the 2D DIGE results, showing downregulation of an αTm isoform to very low levels during immortalization of the BMhTERT-1L culture and robust upregulation during immortalization of BMhTERT-2L cells (Figure 5a, lower panel, and Table 2). Consistent with the immortalized BMhTERT-2L cells, two strong bands were evident in the immunoblot of each of the four immortal BMhTERT clones that repressed $p16^{INK4a}$. The Tm isoform represented by the upper band was strong in only 1 out of 8 BMhTERT cell lines that retained expression of $p16^{INK4a}$ (BM2A7). Together, the immunoblot results for vimentin and αTm highlight the tendency for deregulation of cytoskeletal proteins in $p16^{INK4a}$-negative cells and are in general concordance with the proteomic findings.

Cytoskeletal changes in immortal BMhTERT cells that repressed $p16^{INK4a}$

In light of the deregulated expression of cytoskeletal proteins in immortalized BMhTERT cells, immunofluorescence staining was performed to visualize the cytoskeletal architecture and morphology of BMhTERT and BMECs. Phalloidin and paxillin antibodies were used to stain the actin cytoskeleton and focal adhesions, respectively (Figure 5b). Fluorescence microscopy showed no substantial difference in the cytostructure of early-passage BMhTERT-2 cells and immortal $p16^{INK4a}$-positive BMhTERT-1 cells compared with normal BMECs (Figure 5b, top three panels). These cells all had a fine meshwork of actin fibers, diffusely stained focal adhesions and actin-rich membrane ruffles with a fluid appearance, which was suggestive of motility (Figure 5b). This morphology was also seen in the two $p16^{INK4a}$-positive clones that were examined by immunofluorescence staining (BM2A7 and BM2A2) (Supplementary Figure 2, top two panels). By contrast, the $p16^{INK4a}$-negative immortalized BMhTERT-2 cells had a dense network of thick actin cables, prominent focal adhesions and blunt membrane edges (Figure 5b, bottom panel). The morphologic features of immortalized BMhTERT-2 cells are consistent with a more stable cytoskeleton that is less likely to be amenable to motility and the morphogenic changes required for vessel formation, compared with normal BMECs and $p16^{INK4a}$-positive BMhTERT cells. The $p16^{INK4a}$-negative BMhTERT clones BM2B8 and BM2B12 also had thick actin stress fibers relative to normal BMECs (Supplementary Figure 2, bottom two panels, compared with Figure 5b, top panel). Interestingly the BM2A9 cell line, which was the only $p16^{INK4a}$-negative clone to form vessels in the Matrigel assay (Figure 3), showed a morphology that was more consistent with the $p16^{INK4a}$-positive cells. BM2A9 cells had fine actin-rich membrane ruffles and relatively few dense stress fibers (Supplementary Figure 2, middle panel). Overall, the results from the immunofluorescence staining demonstrate that immortal BMhTERT cells that continued to express $p16^{INK4a}$ invariably retained the cytoskeletal features of normal BMECs and early-passage BMhTERT cells, whereas immortal BMhTERT cells that repressed $p16^{INK4a}$ had a propensity to undergo cytoskeletal changes.

siRNA-mediated repression of $p16^{INK4a}$ in normal BMECs impairs cell motility and vessel formation *in vitro*

To determine whether the impaired capacity of $p16^{INK4a}$-negative BMhTERT cells to undergo morphogenesis and form vessels was directly linked to repression of $p16^{INK4a}$, normal BMECs were transiently transfected with small interfering RNA (siRNA) targeting $p16^{INK4a}$. Repression of $p16^{INK4a}$ in the transfected cells was confirmed by quantitative real-time PCR and immunoblotting (Figures 6a and b). By 24 h after transfection, $p16^{INK4a}$ mRNA levels were depleted to ~10% of the level detected in BMECs transfected with a scrambled siRNA (Sc) (Figure 6a). Protein levels were also very low at the 24-h time point and remained suppressed until 48 h after transfection (Figure 6b). Fluorescence-activated cell sorting analysis confirmed that siRNA-mediated repression of $p16^{INK4a}$ did not alter the expression of VEGF receptors (VEGFR1 and VEGFR2) or the EC adhesion molecules PECAM-1 (CD31) and ICAM-1 (CD54) (Supplementary Table 1).

The ability of the BMECs to form vessels in Matrigel was measured 24 h after siRNA transfection. Microscopic examination and quantitation of the transfected cultures in four independent experiments confirmed that repression of $p16^{INK4a}$ dramatically impaired the ability of BMECs to form vessel-like structures in this assay (Figure 6c). The number of vessels per field was approximately threefold reduced in cultures of $p16^{INK4a}$ siRNA-transfected BMECs when compared with Sc-transfected cultures ($P<0.05$, paired Student's *t*-test) (Figure 6d). Indeed these experiments also revealed a direct correlation between the level of $p16^{INK4a}$ expression and the number vessels formed in this assay ($P<0.01$, Pearson's correlation) (Figure 6e). Overall these data confirm that loss of endogenous $p16^{IN4Ka}$ expression impairs the ability of BMECs to undergo morphogenic differentiation and form vessels.

As the defect in vessel formation by $p16^{INK4a}$-repressed cells could not be attributed to a decreased rate of proliferation or response to mitogens (Figures 2b–d), we investigated the effects

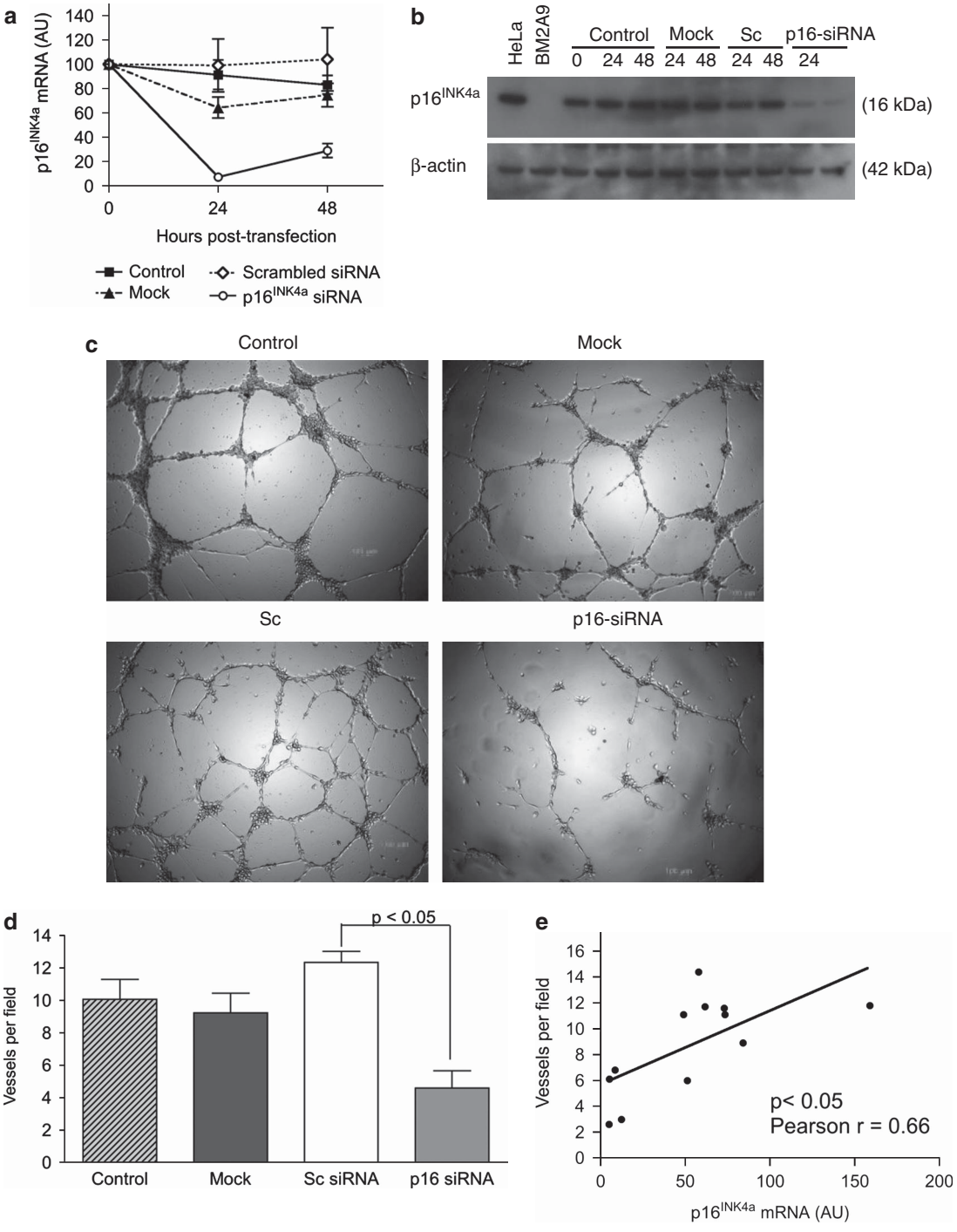

Figure 6. siRNA-mediated repression of $p16^{INK4a}$ in normal BMECs represses vessel formation. Normal BMECs were transfected with an Sc or an siRNA targeting the $p16^{INK4a}$ mRNA (p16-siRNA). (**a**) Quantitative real-time PCR was performed to determine relative expression of $p16^{INK4a}$ mRNA in transfected, mock-transfected and control (non-transfected) BMECs. $p16^{INK4a}$ expression was normalized to β_2-microglobulin and expressed relative to control cells at 0 h. The values are means + s.e.m. calculated from four independent experiments. (**b**) Immunoblot showing the $p16^{INK4a}$ protein in control, mock- and p16-siRNA-transfected BMECs. Actin was used as a loading control. (**c**) siRNA-transfected and control BMECs were seeded onto Matrigel 24 h after transfection. Photomicrographs were taken using a $\times 5$ objective after 6-h incubation in Matrigel. (**d**) Graphical representation of the number of vessel-like structures per field. Values are the average number of vessels per field + s.e.m., enumerated over 10 fields from four independent experiments. The *P*-values were generated by comparison of Sc- and p16-siRNA-transfected BMECs by paired Student's *t*-test. (**e**) Correlation between the number of vessel-like structures versus $p16^{INK4a}$ mRNA expression calculated by Pearson's test.

of $p16^{INK4a}$ repression on random cell motility, a property required by ECs to explore and colonize new areas during the process of angiogenesis. Live-cell imaging over a 6 h period revealed a clear motility defect in BMECs transfected with $p16^{INK4a}$ siRNA. The $p16^{INK4a}$-transfected cells covered a distance that was approximately 30% less than the controls in each of three independent

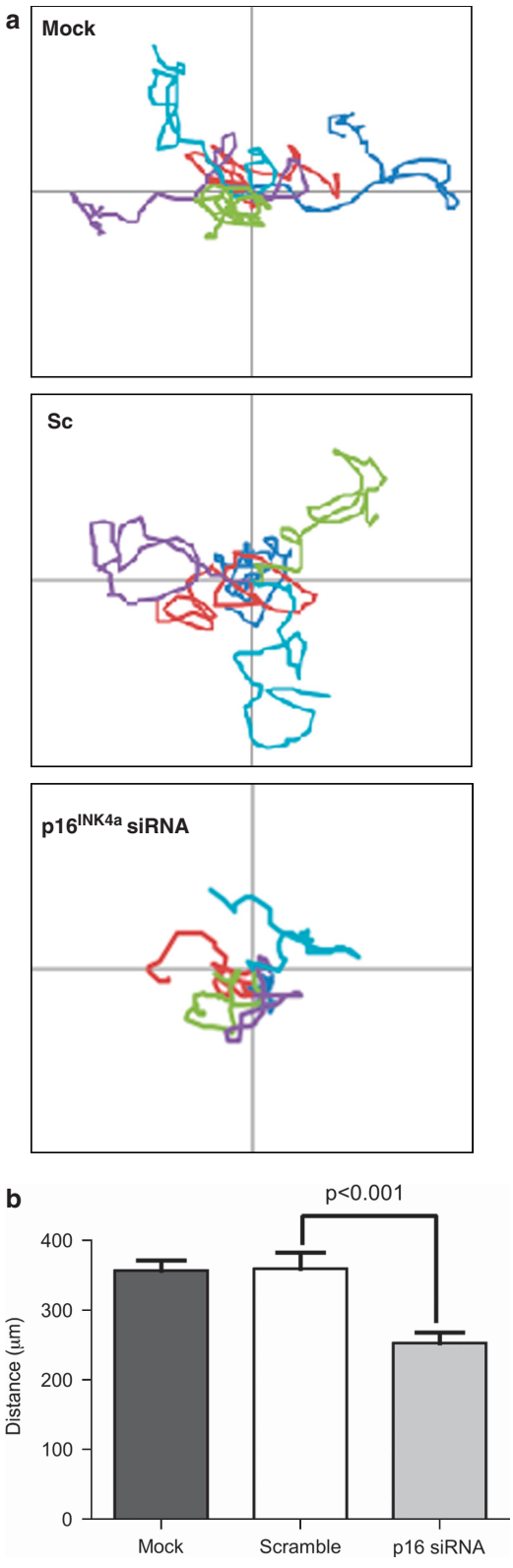

Figure 7. Impaired motility of BMECs following repression of $p16^{INK4a}$. BMECs were split into gelatin-coated plates 24 h after siRNA or mock transfection. Time-lapse video microscopy was initiated 1 h and images were captured over 6 h. (**a**) Representative trajectories of individual BMECs. Five cells from each condition are shown in each graph. (**b**) Graphical representation of the distance travelled by BMECs during the 6-h imaging procedure. The values are means + s.e.m. calculated from at least 25 cells in three independent experiments. $P < 0.001$ by Student's *t*-test.

experiments (Figures 7a and b) ($P < 0.001$, paired Student's *t*-test). These results indicate that defective vessel formation associated with repression of $p16^{INK4a}$ was likely due (at least in part) to an impaired ability to move and explore the surrounding environment.

DISCUSSION

This report reveals novel functional and molecular alterations associated with repression of $p16^{INK4a}$ in human ECs. Using a panel of hTERT-immortalized BMECs, it was shown that the majority of the cell lines that spontaneously repressed $p16^{INK4a}$ were unable to form vessel-like structures *in vitro*. The causal role of $p16^{INK4a}$ silencing in this defect was supported by analysis of normal BMECs subject to siRNA-mediated repression of $p16^{INK4a}$, which confirmed that vessel formation inversely correlated with the level of $p16^{INK4a}$ expression. Time delay video microscopy revealed that $p16^{INK4a}$ siRNA-transfected BMECs also had compromised motility, which would have contributed to the impaired function of these cells in the vessel formation assay. BMhTERT cells that silenced $p16^{INK4a}$ during immortalization had a propensity to accumulate cytoskeletal alterations that were also likely to impact on vessel formation.

Prior to the present study, it was shown that overexpression of $p16^{INK4a}$ in human umbilical vein and microvascular ECs decreased proliferation, impaired migration and abrogated vessel formation *in vitro*.[32] The phenotype described in the report by Alhaja *et al*.[32] illustrates the impaired function of ECs undergoing senescence, a process others have shown to be efficiently induced by overexpression of $p16^{INK4a}$ in human umbilical vein ECs.[33] Independent investigators have also demonstrated very high levels of endogenous $p16^{INK4a}$ and EC dysfunction in ECs subject to stress-induced or replicative senescence.[5,14,34,35] As the level of $p16^{INK4a}$ expressed by $p16^{INK4a}$-positive immortal BMhTERT cells approximated that of early-passage BMECs, our data do not conflict with the report by Alhaja *et al*.[32] Instead the current report, taken together with previous studies of EC senescence, highlight the importance of low levels of $p16^{INK4a}$ for normal EC function and illustrate how either loss of $p16^{INK4a}$ during carcinogenesis or accumulation of $p16^{INK4a}$ during replicative aging may result in EC dysfunction. The effect of $p16^{INK4a}$ expression on EC function is most likely mediated by pRB, which impacts on diverse cell functions by regulating a suite of eight E2F transcriptional repressors and activators, as well as numerous other interacting proteins.[36]

As remodeling of the cytoskeleton has a crucial role in EC motility and morphogenic differentiation,[37] it was notable that the immortalized BMhTERT-2 cell line, which had repressed $p16^{INK4a}$ expression and failed to form vessel structures, had deregulated expression of several cytoskeletal proteins, including vimentin and high-molecular-weight αTm isoforms. Vimentin is an intermediate filament that is required for cytoskeletal stability, and has a key role in cell adhesion and motility.[38,39] The detection of multiple vimentin variants in this study was consistent with vimentin's known propensity for post-translational modification and cleavage.[40,41] The two isoforms detected by MALDI-MS in the current study are consistent with vimentin proteins detected by 2D proteomic analysis of an irradiated EC line.[42] Our proteomic analyses showed that the lower molecular weight isoform (~48 kDa) was reduced during immortalization of both mass cultures, whereas the higher molecular weight isoform (~57 kDa) was less abundant in the mass culture that repressed $p16^{INK4a}$. The apparent ambiguity between the proteomic and immunoblot analyses was most likely a consequence of the different solutions used to isolate and fractionate proteins in the 2D verses one-dimensional gel formats, and/or a reflection of the epitopes detected by the antibody. Irrespective of these differences, our results revealed a general tendency for downregulation of

vimentin isoforms in most immortalized BMhTERT cell lines, which is consistent with the maintenance of a 'young' phenotype in TERT-immortalized ECs, relative to the extreme abundance of this protein in senescent cells.[43,44] Demonstration of downregulation of vimentin during EC immortalization is also a notable finding in relation to the use of this protein as a diagnostic marker for EC tumors and cancers of unknown primary sites.[45]

Tm is a highly conserved actin-binding cytoskeletal constituent that functions in the stabilization of stress fibers in non-muscle cells. The αTm gene encodes at least 10 different isoforms that show varied patterns of expression among different tissues and during development.[46] To date, very little has been published on the regulation and function of Tms in ECs, although post-translational modifications have been observed in human umbilical vein ECs subject to oxidative and shear stresses.[47,48] The current study demonstrated upregulation of a high-molecular-weight αTm gene product in each of the five $p16^{INK4a}$-negative immortal BMhTERT cell lines analyzed in this study. These results are striking in relation to studies that have shown high-molecular-weight Tms have tumor-suppressor properties and are downregulated in experimentally transformed fibroblasts and various human malignancies.[49–54] However, as $p16^{INK4a}$ negative-BMhTERT cells are non-tumorigenic and retain p53 function,[25] our results may have more relevance to a study that showed an association between expression of high-molecular-weight Tms and retarded cell motility in normal and non-transformed, immortal breast epithelial cells.[55] Also relevant to the current report, previous studies implicated αTm as a mediator of anti-angiogenic signals.[56,57] Further studies will be required to fully characterize Tm isoforms expressed in human ECs and to delineate their functions.

BMhTERT cells that silenced $p16^{INK4a}$ during immortalization tended to have more dramatic changes in cytoskeletal proteins as well as cytoarchitectures that had a more rigid appearance compared with normal BMECs and immortal cells that retained $p16^{INK4a}$ expression. While each of the $p16^{INK4a}$-negative cell lines showed abnormalities in both vimentin and αTm, concurrent alteration of these proteins was not detected in any of the $p16^{INK4a}$-positive cell lines, which all retained normal cell morphology. However, the observed alterations in vimentin and αTm did not appear to be directly linked to $p16^{INK4a}$ expression, as changes in either vimentin or αTm were observed in some $p16^{INK4a}$-positive clones and these proteins were not altered by siRNA-mediated downregulation of $p16^{INK4a}$ in normal BMECs (additional data not shown). Paxillin and phalloidin staining confirmed that there were also no morphologic changes immediately induced by siRNA-mediated repression of $p16^{INK4a}$ in BMECs (data not shown). One possible explanation for the accumulation of cytoskeletal changes in BMhTERT clones that silenced $p16^{INK4a}$ by methylation, and the absence of these changes from BMECs transfected with siRNA targeting $p16^{INK4a}$, is that some of the cytoskeletal alterations were a consequence the epigenetic event(s) that orchestrated the methylation of the *CDKN2A* promoter in BMhTERT cells. The clustering of cytoskeletal protein alterations among the $p16^{INK4a}$-negative cells may also reflect a process of selection during immortalization. Based on a previous report that illustrated the importance of an appropriate EC cytoskeletal structure for G_1-to-S-phase progression,[58] we hypothesize that the compound changes in vimentin and αTm may not be permissive for normal cell-cycle progression in cells with the G_1/S checkpoint intact. However, the uncoupling of this checkpoint in $p16^{INK4a}$-negative BMhTERT cells may provide a mechanism for the continued proliferation and eventual immortalization of cells that harbored these cytoskeletal changes. Alternatively, as we have shown that repression of $p16^{INK4a}$ directly impacted on normal BMEC function (motility), it is also possible that the observed alterations in vimentin and/or αTm were compensatory changes required for stability and continued proliferation of BMhTERT cells that lacked expression of $p16^{INK4a}$.

In summary, this report is the first to demonstrate the essential role of low levels of $p16^{INK4a}$ in the maintenance of normal EC function and morphology. This study shows that ECs that repress expression of $p16^{INK4a}$ are prone to defects in motility and morphogenesis, as well as cytoskeletal alterations. As the immortalization process is an essential step in tumorigenesis and $p16^{INK4a}$ is frequently silenced in angiosarcomas, the results from this study provide valuable insight to mechanisms that may contribute to the pathogenesis of aggressive EC-derived malignancies, which feature methylation and/or deletion of the $p16^{INK4a}$ locus.[3,4]

MATERIALS AND METHODS

Cell culture and siRNA transfections

The establishment and immortalization of BMhTERT clones and mass cultures were described previously.[13,25] For all experiments except the growth factor withdrawal study, BMECs and BMhTERT cells were maintained in EC growth medium at 37 °C in a humidified incubator with 5% CO_2.[13] For growth factor withdrawal experiments, the cells were grown using the EGMT-2-MV BulletKitT (Lonza, Mt Waverly, VIC, Australia). siRNA targeting exon-1 (106–126) of the *CDKN2A* gene was designed using the HiPerformance siRNA Design Algorithm (licensed by Novartis, Basal, Switzerland and made available by Qiagen, Doncaster, VIC, Australia). The sequence of siRNA targeting $p16^{INK4a}$ was as follows: sense: 5′-CUGCC CAACGCACCGAAUAtt-3′; antisense: 5′-UAUUCGGUGCGUUGGGCAGcg-3′. The sequence of the control siRNA (Sc) was sense: 5′-CAGUCGCGUUUGCG ACUGGtt-3′; antisense: 5′-CCAGUCGCAAACGCGACUGtt-3′.[59] For siRNA transfections, 2.0×10^6 BMECs were suspended in 100 μl of Nucleofector solution L (Lonza) and transfected with 150 pmole of siRNA (Sigma-Aldrich, St Louis, MO, USA) suspended in Tris-EDTA buffer using program X001 on an Amaxa Biosystems Nucleofector II (Lonza). Transfected BMECs were immediately returned to culture in EC growth medium and incubated at 37 °C under humidified air and 5% CO_2.

MTT proliferation assay

Cells were plated at 3000 per 100 μl EC growth medium per well in a 96-well plate and MTT was added 24 h later. The reaction was stopped 4 h later by addition of 10% sodium dodecyl sulfate (Ameresco, Framinham, MA, USA) in 0.01 M HCl. Optical density was measured at 570 nm using an Amersham Biotrak II Plate Reader (GE Healthcare, Piscataway, NJ, USA).

In vitro vessel formation and random motility assays

Matrigel (BD Biosciences, North Ryde, NSW, Australia) was diluted 1:1 in M199 medium supplemented with 0.1% fetal calf serum, 10 U/ml heparin (Pfizer, New York, NY, USA), 5 ng/ml fibroblast growth factor-β (Sigma-Aldrich), 20 μg/ml Endothelial Cell Growth Factor (Roche, Mannheim, Germany), 10 mg/ml penicillin (Invitrogen, CA, USA), 10 mg/ml streptomycin (Invitrogen) and 29.2 mg/ml glutamine mix (Invitrogen, Mulgrove, VIC, Australia). The Matrigel solution was dispensed into a 24-well plate and incubated for 1 h at 37 °C. BMECs were overlaid onto the Matrigel at 7.5×10^4 cells per well and incubated at 37 °C for 6 h. Vessel-like structures (enclosed polygons) were photographed using the ×5 objective of an Axiovert 200M fluorescent microscope coupled to an AxioCamMR3 camera (Carl Zeiss, Munich, Germany). Ten fields of view were photographed for each condition and the number of vessel-like structures was quantified using the Zeiss AxioVision 4.7 Image Analysis software.

Random motility was assessed 24 h after BMEC transfection by time-lapse microscopy as described previously.[60] Briefly, BMECs were seeded at 2×10^4 cells/ml in 3 ml of EC growth medium per well in 0.1% gelatin-coated six-well plates and incubated at 37 °C under 5% CO_2. Images of at least two fields of view were captured every 5 min for 6 h using the microscope and camera setup described above. At least 25 cells per field of view were tracked over 6 h. Cells undergoing division or apoptosis were

excluded from analyses. Cell motility was quantified using the tracking module of the AxioVision 4.7 software. The persistent random-walk model was used to quantify motility of individual cells.[61]

Quantitative real-time PCR

RNA was extracted using the Qiagen RNeasy Mini kit (Qiagen), followed by reverse transcription using SuperScript III reverse transcriptase (Invitrogen), according to the manufacturer's instructions. Real-time reverse transcription–PCR was performed using the iQ SYBR Green Supermix (Bio-Rad, Hercules, CA, USA), using the MyiQ Real Time PCR Machine (Bio-Rad), applying the following cycling conditions: 95 °C for 10 min; followed by 40 cycles of 95 °C for 30 s, 64 °C for 30 s, 72 °C for 1 min; and a final 10-min extension step at 72 °C. The primer sequences were as follows: $p16^{INK4a}$ forward 5′-ATGGAGCCTTCGGCTGACTGGC-3′, $p16^{INK4a}$ reverse 5′-CTGCCCA TCATCATGACCTGGA-3′; β_2-microglobulin forward 5′-CTCGCGCTACTCT CTCTTTCT-3′, β_2-microglobulin reverse 5′-TACATGTCTCGATCCCACTTAA CTAT-3′.

2DDIGE and MALDI-MS analysis

The methods used for 2DDIGE and identification of differentially expressed proteins by MALDI-MS were described previously.[62] Briefly, mixtures of 50 μg of Cy3- and Cy5-labeled cell lysates, plus 50 μg of a Cy2-labeled internal standard (comprised of mixtures of each sample), were run on six 2DDIGE gels (Table 1) using the Ettan IPGphor IEF system (GE Healthcare, Giles, UK), using Immobiline DryStrips (pH 4–7). The first-dimension gels were run at 300 V for 3 h, 100 V for 6 h, 8000 V for 3 h and 8000 V for 4.4 h. The samples were then run in the second dimension on 12.5% polyacrylamide gels using an Ettan DALT six apparatus (GE Healthcare, Hong Kong, China) at 1.5 W. Protein spots were detected using the Typhoon imager (GE Healthcare) and statistical analysis of differential protein abundance was performed using the DeCyder 2D software V4.0, using the Cy2-labeled reference sample used as a normalization control. Protein spots of interest were excised from gels stained with SYPRO Ruby. MALDI-MS analysis was performed using an Applied Biosystems 4700 Proteomics Analyzer at the Australian Proteome Analysis Facility. MS data were exported to the Mascot database search program (Matrix Science Ltd, London, UK) and searched against *Homo sapiens* entries in the SwissProt database.

Immunoblot analysis

Proteins were extracted in buffer containing 10 mM Tris (pH 8.0), 150 mM NaCl, 1 mM EDTA, 1% Nonidet P-40 and 1% protease inhibitor (Sigma-Aldrich) for 30 min, then separated on a NuPAGENovexBis–Tris 4–12% 1.0 Mini Gel (Invitrogen) and transferred onto a polyvinylidene fluoride membrane (Millipore, Kilsyth, VIC, Australia). The membranes were blocked with 5% skim milk in Tris-buffered saline and hybridized with primary antibodies, followed by a horseradish peroxidase-labeled secondary antibody (GE Healthcare) and visualized using the Pierce ECL Western Blotting Substrate (Thermo-Fisher Scientific, North Ryde, NSW, Australia). The primary antibodies were $p16^{INK4a}$ (BD Biosciences), vimentin (V9; Chemicon, Boronia, VIC, Australia), GSTPi (2G6-F6; Abnova, Taipai, Taiwan), HSCL1 (clone 3D5; Abnova Taipai), αTm exon-9 (provided by Dr Galina Schevzov, University of New South Wales, Australia)[63] and β-actin (Sigma-Aldrich).

Immunofluorescence staining

BMECs and BMhTERT cells were seeded at 2.5×10^4 cells/ml on 0.1% gelatin-coated chamber slides. Twenty-four hours later, the cells were stained with paxillin antibody for visualization of focal adhesions (green), phalloidin–Alexa 568 (red) for actin and DAPI (4′,6-diamidino-2-phenylindole) (blue). The stained cells were photographed under oil immersion using the ×63 objective of an Axiovert 200M fluorescent microscope coupled to an AxioCamMR3 camera (Carl Zeiss).

CONFLICT OF INTEREST

The authors declare no conflict of interest.

ACKNOWLEDGEMENTS

We thank Dr Galina Schevzov and Professor Peter Gunning for provision of the Tm antibody and helpful discussion. Children's Cancer Institute Australia for Medical Research is affiliated with the University of New South Wales and Sydney Children's Hospital. This research was facilitated by access to the Australian Proteome Analysis Facility established under the Australian Government's Major National Research Facilities Program. *Funding*: National Health and Medical Research Council (KLM Career Development Award ID no. 510378; MK Senior Research Fellowship ID no. 568611), New South Wales Cancer Council (KLM ID no. 07-14) and Cancer Institute New South Wales (KLM Career Development and Support Fellowship ID no. 07-CDF-1/23; EP Early Career Research Fellowship ID no. 07/ECF/1-21).

REFERENCES

1 Bell CD. Endothelial cell tumors. *Microsc Res Tech* 2003; **60**: 165–170.
2 Young RJ, Brown NJ, Reed MW, Hughes D, Woll PJ. Angiosarcoma. *Lancet Oncol* [Research Support, Non-US Gov't; Review] 2010; **11**: 983–991.
3 Tannapfel A, Weihrauch M, Benicke M, Uhlmann D, Hauss J, Wrbitzky R *et al.* p16INK4A-alterations in primary angiosarcoma of the liver. *J Hepatol* 2001; **35**: 62–67.
4 Weihrauch M, Markwarth A, Lehnert G, Wittekind C, Wrbitzky R, Tannapfel A. Abnormalities of the ARF–p53 pathway in primary angiosarcomas of the liver. *Hum Pathol* 2002; **33**: 884–892.
5 Wagner M, Hampel B, Bernhard D, Hala M, Zwerschke W, Jansen-Durr P. Replicative senescence of human endothelial cells *in vitro* involves G_1 arrest, polyploidization and senescence-associated apoptosis. *Exp Gerontol* 2001; **36**: 1327–1347.
6 Serrano M, Hannon GJ, Beach D. A new regulatory motif in cell-cycle control causing specific inhibition of cyclin D/CDK4. *Nature* [Research Support, Non-US Gov't; Research Support, US Gov't, PHS] 1993; **366**: 704–707.
7 Spike BT, Dirlam A, Dibling BC, Marvin J, Williams BO, Jacks T *et al.* The Rb tumor suppressor is required for stress erythropoiesis. *EMBO J* [Research Support, Non-US Gov't] 2004; **23**: 4319–4329.
8 Milyavsky M, Shats I, Cholostoy A, Brosh R, Buganim Y, Weisz L *et al.* Inactivation of myocardin and p16 during malignant transformation contributes to a differentiation defect. *Cancer Cell* 2007; **11**: 133–146.
9 Hernando E, Nahle Z, Juan G, Diaz-Rodriguez E, Alaminos M, Hemann M *et al.* Rb inactivation promotes genomic instability by uncoupling cell cycle progression from mitotic control. *Nature* 2004; **430**: 797–802.
10 Urashima M, Teoh G, Akiyama M, Yuza Y, Anderson KC, Maekawa K. Restoration of p16INK4A protein induces myogenic differentiation in RD rhabdomyosarcoma cells. *Br J Cancer* [Research Support, Non-US Gov't] 1999; **79**: 1032–1036.
11 Hanahan D, Weinberg RA. Hallmarks of cancer: the next generation. *Cell* [Research Support, NIH, Extramural; Review] 2011; **144**: 646–674.
12 Hsiao R, Sharma HW, Ramakrishnan S, Keith E, Narayanan R. Telomerase activity in normal human endothelial cells. *Anticancer Res* 1997; **17**: 827–832.
13 MacKenzie KL, Franco S, Naiyer AJ, May C, Sadelain M, Rafii S *et al.* Multiple stages of malignant transformation of human endothelial cells modelled by co-expression of telomerase reverse transcriptase, SV40T antigen and oncogenic N-ras. *Oncogene* 2002; **21**: 4200–4211.
14 Yang J, Chang E, Cherry AM, Bangs CD, Oei Y, Bodnar A *et al.* Human endothelial cell life extension by telomerase expression. *J Biol Chem* [Research Support, Non-US Gov't; Research Support, US Gov't, PHS] 1999; **274**: 26141–26148.
15 Chang E, Harley CB. Telomere length and replicative aging in human vascular tissues. *Proc Natl Acad Sci USA* 1995; **92**: 11190–11194.
16 d'Adda di Fagagna F, Reaper PM, Clay-Farrace L, Fiegler H, Carr P, Von Zglinicki T *et al.* A DNA damage checkpoint response in telomere-initiated senescence. *Nature* 2003; **426**: 194–198.
17 Alcorta DA, Xiong Y, Phelps D, Hannon G, Beach D, Barrett JC. Involvement of the cyclin-dependent kinase inhibitor p16(INK4a) in replicative senescence of normal human fibroblasts. *Proc Natl Acad Sci USA* 1996; **93**: 13742–13747.
18 Hara E, Smith R, Parry D, Tahara H, Stone S, Peters G. Regulation of p16CDKN2 expression and its implications for cell immortalization and senescence. *Mol Cell Biol* 1996; **16**: 859–867.
19 Jacobs JJ, de Lange T. Significant role for p16INK4a in p53-independent telomere-directed senescence. *Curr Biol* 2004; **14**: 2302–2308.
20 Crawford YG, Gauthier ML, Joubel A, Mantei K, Kozakiewicz K, Afshari CA *et al.* Histologically normal human mammary epithelia with silenced p16(INK4a) overexpress COX-2, promoting a premalignant program. *Cancer Cell* [Research Support, Non-US Gov't; Research Support, US Gov't, Non-PHS; Research Support, US Gov't, PHS] 2004; **5**: 263–273.
21 Romanov SR, Kozakiewicz BK, Holst CR, Stampfer MR, Haupt LM, Tlsty TD. Normal human mammary epithelial cells spontaneously escape senescence and acquire genomic changes. *Nature* 2001; **409**: 633–637.

22 Soler D, Genesca A, Arnedo G, Egozcue J, Tusell L. Telomere dysfunction drives chromosomal instability in human mammary epithelial cells. *Genes Chromosomes Cancer* 2005; **44**: 339 - 350.
23 Venetsanakos E, Mirza A, Fanton C, Romanov SR, Tlsty T, McMahon M. Induction of tubulogenesis in telomerase-immortalized human microvascular endothelial cells by glioblastoma cells. *Exp Cell Res* 2002; **273**: 21 - 33.
24 O'Hare MJ, Bond J, Clarke C, Takeuchi Y, Atherton AJ, Berry C *et al.* Conditional immortalization of freshly isolated human mammary fibroblasts and endothelial cells. *Proc Natl Acad Sci USA* 2001; **98**: 646 - 651.
25 Wen VW, Wu K, Baksh S, Hinshelwood RA, Lock RB, Clark SJ *et al.* Telomere-driven karyotypic complexity concurs with p16INK4a inactivation in TP53-competent immortal endothelial cells. *Cancer Res* 2006; **66**: 10691 - 10700.
26 Gil-Benso R, Lopez-Gines C, Soriano P, Almenar S, Vazquez C, Llombart-Bosch A. Cytogenetic study of angiosarcoma of the breast. *Genes Chromosomes Cancer* [Case Reports] 1994; **10**: 210 - 212.
27 Kindblom LG, Stenman G, Angervall L. Morphological and cytogenetic studies of angiosarcoma in Stewart - Treves syndrome. *Virchows Arch A Pathol Anat Histopathol* [Case Reports; Research Support, Non-US Gov't] 1991; **419**: 439 - 445.
28 Mandahl N, Jin YS, Heim S, Willen H, Wennerberg J, Biorklund A *et al.* Trisomy 5 and loss of the Y chromosome as the sole cytogenetic anomalies in a cavernous hemangioma/angiosarcoma. *Genes Chromosomes Cancer* 1990; **1**: 315 - 316.
29 Schuborg C, Mertens F, Rydholm A, Brosjo O, Dictor M, Mitelman F *et al.* Cytogenetic analysis of four angiosarcomas from deep and superficial soft tissue. *Cancer Genet Cytogenet* 1998; **100**: 52 - 56.
30 Zu Y, Perle MA, Yan Z, Liu J, Kumar A, Waisman J. Chromosomal abnormalities and p53 gene mutation in a cardiac angiosarcoma. *Appl Immunohistochem Mol Morphol* [Case Reports] 2001; **9**: 24 - 28.
31 Baumhoer D, Gunawan B, Becker H, Fuzesi L. Comparative genomic hybridization in four angiosarcomas of the female breast. *Gynecol Oncol* 2005; **97**: 348 - 352.
32 Alhaja E, Adan J, Pagan R, Mitjans F, Cascallo M, Rodriguez M *et al.* Anti-migratory and anti-angiogenic effect of p16: a novel localization at membrane ruffles and lamellipodia in endothelial cells. *Angiogenesis* [Research Support, Non-US Gov't] 2004; **7**: 323 - 333.
33 Chen J, Huang X, Halicka D, Brodsky S, Avram A, Eskander J *et al.* Contribution of p16INK4a and p21ClP1 pathways to induction of premature senescence of human endothelial cells: permissive role of p53. *Am J Physiol Heart Circ Physiol* 2006; **290**: H1575 - H1586.
34 Minamino T, Miyauchi H, Yoshida T, Ishida Y, Yoshida H, Komuro I. Endothelial cell senescence in human atherosclerosis: role of telomere in endothelial dysfunction. *Circulation* 2002; **105**: 1541 - 1544.
35 Minamino T, Miyauchi H, Yoshida T, Tateno K, Komuro I. The role of vascular cell senescence in atherosclerosis: antisenescence as a novel therapeutic strategy for vascular aging. *Curr Vasc Pharmacol* 2004; **2**: 141 - 148.
36 Chinnam M, Goodrich DW. RB1, development, and cancer. *Curr Top Dev Biol* [Research Support, NIH, Extramural; Review] 2011; **94**: 129 - 169.
37 Lamalice L, Le Boeuf F, Huot J. Endothelial cell migration during angiogenesis. *Circ Res* [Research Support, US Gov't, Non-PHS; Review] 2007; **100**: 782 - 794.
38 Ivaska J, Pallari HM, Nevo J, Eriksson JE. Novel functions of vimentin in cell adhesion, migration, and signaling. *Exp Cell Res* [Review] 2007; **313**: 2050 - 2062.
39 Eckes B, Dogic D, Colucci-Guyon E, Wang N, Maniotis A, Ingber D *et al.* Impaired mechanical stability, migration and contractile capacity in vimentin-deficient fibroblasts. *J Cell Sci* [Research Support, Non-US Gov't; Research Support, US Gov't, Non-PHS; Research Support, US Gov't, PHS] 1998; **111** (Pt 13): 1897 - 1907.
40 Eriksson JE, He T, Trejo-Skalli AV, Harmala-Brasken AS, Hellman J, Chou YH *et al.* Specific *in vivo* phosphorylation sites determine the assembly dynamics of vimentin intermediate filaments. *J Cell Sci* [Research Support, Non-US Gov't] 2004; **117**(Pt 6): 919 - 932.
41 Valgeirsdottir S, Claesson-Welsh L, Bongcam-Rudloff E, Hellman U, Westermark B, Heldin CH. PDGF induces reorganization of vimentin filaments. *J Cell Sci* 1998; **111**(Pt 14): 1973 - 1980.
42 Nylund R, Leszczynski D. Proteomics analysis of human endothelial cell line EA.hy926 after exposure to GSM 900 radiation. *Proteomics* [Research Support, Non-US Gov't] 2004; **4**: 1359 - 1365.
43 Wang E. Are cross-bridging structures involved in the bundle formation of intermediate filaments and the decrease in locomotion that accompany cell aging? *J Cell Biol* [Research Support, US Gov't, PHS] 1985; **100**: 1466 - 1473.
44 Nishio K, Inoue A, Qiao S, Kondo H, Mimura A. Senescence and cytoskeleton: overproduction of vimentin induces senescent-like morphology in human fibroblasts. *Histochem Cell Biol* [Research Support, Non-US Gov't] 2001; **116**: 321 - 327.
45 Koch M, Nielsen GP, Yoon SS. Malignant tumors of blood vessels: angiosarcomas, hemangioendotheliomas, and hemangiopericytomas. *J Surg Oncol* [Review] 2008; **97**: 321 - 329.
46 Gunning PW, Schevzov G, Kee AJ, Hardeman EC. Tropomyosin isoforms: divining rods for actin cytoskeleton function. *Trends Cell Biol* [Research Support, Non-US Gov't; Review] 2005; **15**: 333 - 341.
47 Houle F, Poirier A, Dumaresq J, Huot J. DAP kinase mediates the phosphorylation of tropomyosin-1 downstream of the ERK pathway, which regulates the formation of stress fibers in response to oxidative stress. *J Cell Sci* 2007; **120**(Pt 20): 3666 - 3677.
48 Huang B, Chen SC, Wang DL. Shear flow increases *S*-nitrosylation of proteins in endothelial cells. *Cardiovasc Res* [Research Support, Non-US Gov't] 2009; **83**: 536 - 546.
49 Prasad GL, Fuldner RA, Cooper HL. Expression of transduced tropomyosin 1 cDNA suppresses neoplastic growth of cells transformed by the ras oncogene. *Proc Natl Acad Sci USA* [In Vitro] 1993; **90**: 7039 - 7043.
50 Hendricks M, Weintraub H. Tropomyosin is decreased in transformed cells. *Proc Natl Acad Sci USA* [Research Support, US Gov't, PHS] 1981; **78**: 5633 - 5637.
51 Franzen B, Linder S, Uryu K, Alaiya AA, Hirano T, Kato H *et al.* Expression of tropomyosin isoforms in benign and malignant human breast lesions. *Br J Cancer* [Comparative Study; Research Support, Non-US Gov't] 1996; **73**: 909 - 913.
52 Bhattacharya B, Prasad GL, Valverius EM, Salomon DS, Cooper HL. Tropomyosins of human mammary epithelial cells: consistent defects of expression in mammary carcinoma cell lines. *Cancer Res* [In Vitro] 1990; **50**: 2105 - 2112.
53 Hughes JA, Cooke-Yarborough CM, Chadwick NC, Schevzov G, Arbuckle SM, Gunning P *et al.* High-molecular-weight tropomyosins localize to the contractile rings of dividing CNS cells but are absent from malignant pediatric and adult CNS tumors. *Glia* [Research Support, Non-US Gov't] 2003; **42**: 25 - 35.
54 Wang FL, Wang Y, Wong WK, Liu Y, Addivinola FJ, Liang P *et al.* Two differentially expressed genes in normal human prostate tissue and in carcinoma. *Cancer Res* [Research Support, Non-US Gov't] 1996; **56**: 3634 - 3637.
55 Zheng Q, Safina A, Bakin AV. Role of high-molecular weight tropomyosins in TGF-beta-mediated control of cell motility. *Int J Cancer* [Research Support, NIH, Extramural; Research Support, US Gov't, Non-PHS] 2008; **122**: 78 - 90.
56 MacDonald NJ, Shivers WY, Narum DL, Plum SM, Wingard JN, Fuhrmann SR *et al.* Endostatin binds tropomyosin. A potential modulator of the antitumor activity of endostatin. *J Biol Chem* 2001; **276**: 25190 - 25196.
57 Zhang JC, Donate F, Qi X, Ziats NP, Juarez JC, Mazar AP *et al.* The antiangiogenic activity of cleaved high molecular weight kininogen is mediated through binding to endothelial cell tropomyosin. *Proc Natl Acad Sci USA* [Research Support, US Gov't, Non-PHS; Research Support, US Gov't, PHS] 2002; **99**: 12224 - 12229.
58 Huang S, Chen CS, Ingber DE. Control of cyclin D1, p27(Kip1), and cell cycle progression in human capillary endothelial cells by cell shape and cytoskeletal tension. *Mol Biol Cell* [Research Support, Non-US Gov't; Research Support, US Gov't, PHS] 1998; **9**: 3179 - 3193.
59 Ling X, Li F. Silencing of antiapoptotic survivin gene by multiple approaches of RNA interference technology. *Biotechniques* [Comparative Study; Evaluation Studies; Research Support, Non-US Gov't; Validation Studies] 2004; **36**: 450 - 454; 6 - 60.
60 Pasquier E, Sinnappan S, Munoz MA, Kavallaris M. ENMD-1198, a new analogue of 2-methoxyestradiol, displays both antiangiogenic and vascular-disrupting properties. *Mol Cancer Ther* [Research Support, Non-US Gov't] 2010; **9**: 1408 - 1418.
61 Kouvroukoglou S, Dee KC, Bizios R, McIntire LV, Zygourakis K. Endothelial cell migration on surfaces modified with immobilized adhesive peptides. *Biomaterials* [Research Support, US Gov't, Non-PHS] 2000; **21**: 1725 - 1733.
62 Verrills NM, Liem NL, Liaw TY, Hood BD, Lock RB, Kavallaris M. Proteomic analysis reveals a novel role for the actin cytoskeleton in vincristine resistant childhood leukemia–an *in vivo* study. *Proteomics* 2006; **6**: 1681 - 1694.
63 Schevzov G, Vrhovski B, Bryce NS, Elmir S, Qiu MR, O'Neill G M *et al.* Tissue-specific tropomyosin isoform composition. *J Histochem Cytochem* [Research Support, Non-US Gov't] 2005; **53**: 557 - 570.

Supplementary Information accompanies the paper on the Oncogene website (http://www.nature.com/onc)